Journal of Solid State Chemistry 182 (2009) 677–684

Contents lists available at ScienceDirect

Journal of Solid State Chemistry

journal homepage: www.elsevier.com/locate/jssc

# Fabrication and morphology control of $BaWO_4$ thin films by microwave assisted chemical bath deposition

Rui Wang, Chen Liu, Jia Zeng, KunWei Li, Hao Wang *

*The College of Materials Science and Engineering, Beijing University of Technology, Beijing 100124, PR China*

ARTICLE INFO

*Article history:*
Received 8 September 2008
Received in revised form
1 December 2008
Accepted 17 December 2008
Available online 31 December 2008

*Keywords:*
$BaWO_4$
Thin films
Microwave assisted chemical bath deposition

ABSTRACT

Highly crystallized barium tungstate ($BaWO_4$) thin films with dumbbell-like, kernel-like, bowknot-like and cauliflower-like microstructure were synthesized from an aqueous solution containing barium nitrate, ethylenediamine tetraacetate acid disodium and sodium tungstate, via mild microwave assisted chemical bath deposition process. The resulting $BaWO_4$ films with different morphologies were characterized by X-ray diffraction spectrum, scanning electron microscope, Raman and photoluminescence spectra. The results indicate that the morphologies of final products significantly depend on the reaction conditions including the reaction time, the initial concentration of precursor reagent and the physicochemical characteristics of the substrates. Furthermore, the oriented aggregation mechanism is proposed as a possible formation mechanism of the films with specific morphologies.



## 1. Introduction

The shape, phase, and size of inorganic nanocrystals and microcrystals are important elements in varying their electrical, optical, and other properties [1–5], so rational control over these elements has become a hot research topic in recent years [6]. Many efforts have been made in the controllable methods for synthesizing nano- and microcrystals with specific size and morphology, in order to contrive new materials and devices in various fields such as catalysis, medicine, electronics, ceramics, pigments, cosmetics [7–10], etc.

As an one-step, environment-friendly and low-energy-consumption aqueous technique, chemical bath deposition (CBD) has been wildly applied for depositing large-area semiconductor films with particular shape, orientation and thickness [11,12]. In fact, microwave assisted chemical bath deposition (MA-CBD) is a fascinating film preparation method, since it combines all the merit of CBD and the high time efficiency with enhanced film adherence [13]. It is generally accepted that constant reorientation caused by the response of electric dipoles materials to mutative electric field creates friction and collisions between molecules, which subsequently generates heat. In the case of applying microwave irradiation in chemical bath, the fast, homogeneous heating and the formation of active spots on the conducting substrate can lead to a faster and more simultaneous heterogeneous nucleation on the supporting surface than conventional heating [14–17]. However, Only a few kinds of thin film materials have been successfully deposited by MA-CBD until now, such as ZnO [18], ZnS,CdS [19], $TiO_2$ [20], and Eu:$YVO_4$ [21].

There has been a recent highlighted interesting in scheelite structured $BaWO_4$ which is a high quality material in electro-optical manufacture. Its interesting emission of blue luminescence and stimulated Raman scattering (SRS) properties render $BaWO_4$ as a suitable candidate for the design of solid-state lasers that can emit radiation within a specific spectral region. Also, $BaWO_4$ can be used for medical laser treatment applications, up-conversion fiber lasers, and analogous spectroscopic [22–24]. Various techniques has been employed to synthesize $BaWO_4$ crystals, i.e., Czochralski method for bulk $BaWO_4$ [25], micro-emulsions and hydrothermal method for nano- and micro-powder (nanowire [26], cylinders, rods [27], hollow sphere [28], double-taper, scissors, fasciculus, flower, shuttle [29] etc.); It is generally accepted that a thin film phosphor has superior resolution compared with the powders because of their inherently smaller grain size and less lateral scattering. However, less study focus on the preparation of those films. And the film deposition methods mainly fasten on chemical vapor deposition (CVD) [30], evaporation [31], sputtering evaporation [32], and dip coating process [33]. All of these methods are highly energy consuming and inevitably destroy the film morphology due to high temperatures above 500 °C [34]. Recently, Yoshimura et al. successfully prepared $BaWO_4$ film by some soft solution process, such as hydrothermal [35], electrochemical [35,36] and hydrothermal–electrochemical [35] deposition. However, up to now, little focus has been exerted to the controllable morphology of $BaWO_4$ thin film. In this paper, we introduce a facile and fast microwave route to obtain highly

* Corresponding author. Fax: +86 10 67392445.
*E-mail address:* haowang@bjut.edu.cn (H. Wang).

0022-4596/$ - see front matter © 2009 Elsevier Inc. All rights reserved.
doi:10.1016/j.jssc.2008.12.014

crystallized uniform $BaWO_4$ films with controllable morphology and orientation on glass and FTO glass barely within 25 min. Studies found that some related experimental parameters including the reaction time, the initial concentration of the precursor reagent and the property of substrate had great influences on the morphologies of films. By carefully controlling these experimental parameters, $BaWO_4$ thin films consist of dumbbell-like, kernel-like, bowknot-like, and cauliflower-like microstructure can be successfully obtained, respectively. This method may satisfy the requirements of thin films with different morphologies and orientation in a fast and energy saving route, and provide important theoretical reference to the controlled synthesis of other inorganic thin films.

## 2. Experimental section

The $BaWO_4$ films were deposited on the commercial ($1.5 \times 1 \times 0.1$ cm) microscope glass slides and ($1.5 \times 1 \times 0.2$ cm) F: $SnO_2$ (FTO) coated glass substrates. Before deposition, the substrates were cleaned by ultrasonic treatment in toluene, acetone, and ethanol in turn, rinsed with deionized water, and then dried in air. All reagents were analytical grade and used without further purification. In a typical procedure, $Ba(NO_3)_2$ and ethylenediamine tetraacetate acid disodium salt (EDTA-2Na) solutions were mixed in a 150 ml beaker with constant stirring. The pH value of the mixed solution was adjusted to 8 with NaOH. Then, under continuous stirring, the $Na_2WO_4 \cdot 2H_2O$ solution was put into the former beaker in the molecular ratio of $Ba^{2+}$: $EDTA^{2-}$: $WO_4^{2-} = 1:1:1$, and the concentration of these species was defined as the precursor concentration. By continuous stirring, the solution became clear and homogenous. Then the pre-treated substrates were floated on the surface of the above solution to farthest facilitate heterogeneous nucleation on the substrate surface [21]. The solution was then placed in a domestic microwave oven of 2.45 GHz and a maximum power of 700 W, and the reaction was performed under ambient air for different times with 17% power export. All experiments were carried out initially at room temperature (about 20 °C) without further temperature control. After deposition, the films were washed by deionized water and dried in air.

The X-ray diffraction (XRD) analysis was performed on a Bruker Advance D8 diffractometer equipped with graphite-monochromatized Cu$K\alpha$ radiation ($\lambda = 1.54062$). A scanning rate of 0.1/s was used to record the pattern in the range of 10–70°. Scanning electron microcopy (SEM) images were taken on a Hitachi S-3500N scanning electron microscope. Raman spectra were recorded on a JY-HORIBA T64000 spectrometer at room temperature and with an excitation wavelength of 514 nm. Photoluminescence (PL) spectra were measured on a SLM48000DSCF/AB2 fluorescence spectrometer made by American SLM Inc. at room temperature.

## 3. Results

### 3.1. Characterizations of films deposited on glass substrate

Fig. 1 shows the XRD patterns of the as-prepared films on glass substrates at different precursor concentration with the same pH value (pH = 8) and reaction time (25 min). The diffraction peaks of the products can be all indexed to a pure tetragonal scheelite structure with cell parameters $a = 5.61$ and $c = 12.70$ Å, which are in good agreement with the literature values (JCPDS Card Number 43-0646). However, the relative peak intensity of the four films varies significantly, which indicates different crystallinity. The

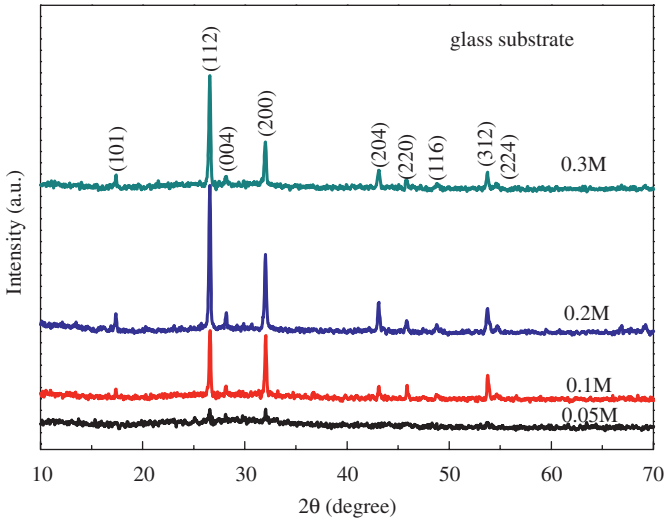


**Fig. 1.** XRD patterns of the as-prepared films on glass substrate at different precursor concentration with the same pH value (pH = 8) and reaction time (25 min).

samples prepared at 0.1–0.3 M show better crystallization than the one made at 0.05 M. No noticeable impurities can be detected. These XRD patterns indicate that well-crystallized $BaWO_4$ films can be easily prepared under the current synthetic conditions. However, if oven heating is employed instead of microwave heating, nearly nothing can be obtained on the substrates within 25 min. According to our related work, if oven heating was employed, at least 12 h was indispensable to achieve the same crystallinity of the samples which deposited within 25 min of microwave heating at the same concentration level. The results indicate that sluggish kinetics of oven heating can be overcome by using microwave heating, which enhances the reaction rate considerably.

The morphologies of these films were observed by SEM. Fig. 2a shows that the film prepared at 0.05 M is composed of symmetrical four sides kernel-like crystals with dimension of 3–4 μm in length and 0.8–1 μm in width. At a precursor concentration of 0.1 M, a few tiny quartered pricks appear at both ends of the four sides kernel-like crystals and the length of the crystals increases to about 8 μm (Fig. 2b) with a slight decrease in the films density. New nucleus and growth elements tend to gather on the existent "shaft" rather than the bare glass substrate [37]. If the precursor concentration further increased to 0.2 M, the two ends of the products further luxuriate and the film density comes up as shown in Fig. 2c. By the concentration added to 0.3 M, the microstructure of the film turns out to be perfect multilayer bowknot-like microcrystal (the insert of Fig. 2d). However, the density of this film decreases again, which maybe attribute to the poor grasping ability of glass substrate since it was floating on the solution surface.

### 3.2. Characterizations of films deposited on FTO coated substrate

The $BaWO_4$ films were also deposited on F: $SnO_2$ (FTO) coated substrates at the same precursor concentration as on glass substrates. The SEM images shown in Fig. 3 clearly reveal the crystallite structures of $BaWO_4$ films obtained from the alkalescent aqueous solution (pH = 8) with various precursor concentration under microwave irradiation for 25 min. The low magnification images (Fig. 3a, c, e, g) indicate the high yield of uniform $BaWO_4$ microcrystals morphologies at each level of precursor concentration. The high magnification images (Fig. 3b,

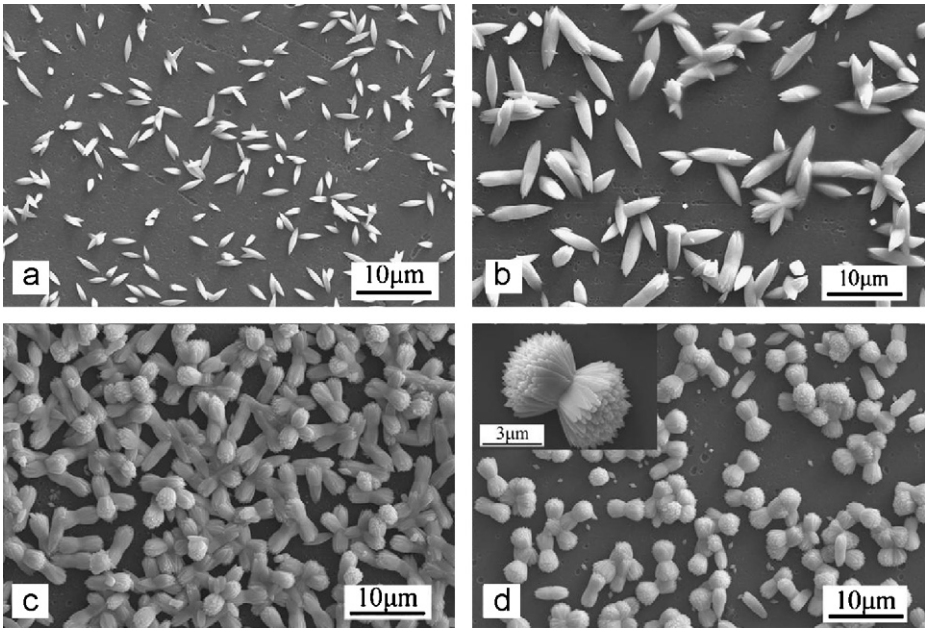


**Fig. 2.** SEM morphologies of the films on glass substrate at different precursor concentration. ($[Ba^{2+}] = [EDTA^{2-}] = [WO_4^{2-}]$ = (a) 0.05 M; (b) 0.1 M; (c) 0.2 M; (d) 0.3 M). pH = 8; 25 min.

d, f, h) demonstrate the evolution process from typical four sides kernel-like to multilayer bowknot-like microstructures. It can be seen that the particular microstructures of the films deposited on both glass and FTO substrate at the same precursor solution concentration (0.05–0.2 M) are extremely alike, while the film on FTO substrate always exhibits an increased density and perpendicular growth tendency by forming quite a lot tetragonal prick on the substrate. When the concentration increased to 0.3 M, film deposited on FTO substrate shows compact and uniform cauliflower-like microcrystals instead of the multilayer bowknot-like ones lied on the glass.

### 3.3. Effect of reaction time

The films obtained in 0.3 M precursor concentration were chosen as a research object for reaction time because of its rather complicated cauliflower-like morphology. As shown in Fig. 4a, c, dumbbell-like crystals appear after 2 and 6 min, respectively. As shown in Fig. 4b, d the typical dumbbell-like crystal with many protuberances on its harsh surface probably is the rudiment of cauliflower-like crystal. If the reaction time further increases to 16 min, the fine edges and corners of cauliflower structure emerge (in Fig. 4e). By the reaction time of 25 min, the cauliflower-like microstructure comprising $BaWO_4$ tetragonal prick subunits is finally formed, as shown in Fig. 4f.

### 3.4. Effect of the pH value

To study the influence of pH values on the morphologies of the products, we also performed the experiments by changing the pH values. When the pH value is adjusted to 7, precipitation promptly appeared, since the $Ba^{2+}$ is not chelated well, no film could be obtained on the substrate. However, when the pH value of the reaction system increased to 13 while keeping the same precursor concentration and reaction time, similar morphology as pH = 8 is observed. Fig. 5 shows typical SEM image of $BaWO_4$ film deposited in the strong alkali solution when other conditions are the same as the sample shown in Fig. 2d. Compared with the films obtained in the solution (pH = 8), similar evolution of shape and crystal size of the film can be observed. Changing the pH values of precursor solution to other pH values in alkalescent solution gave the similar results, which suggests that the variation of pH values have no noticeable influence on the crystallization and the morphology evolution of $BaWO_4$ films.

### 3.5. Raman spectroscopy and PL properties

Optical properties of our synthesized films are also investigated. Fig. 6 shows a typical Raman spectrum of the as-prepared film which exhibits typical Raman bands attributed to crystalline $BaWO_4$ [38]. Films deposited on other conditions exhibit the similar spectra. According to the reported literature, the vibrational modes of isolated $WO_4$ tetrahedron can be separated into internal, external translational, and rotational modes. As shown in Fig. 6, bands at 926, 831, 795, 343, 331 and 191 $cm^{-1}$ originate from the different vibrational modes, including $\upsilon_1(A_g)$, $\upsilon_3(B_g)$, $\upsilon_3(E_g)$, $\upsilon_4(B_g)$, $\upsilon_2(B_g)$ and $\upsilon_{f.r.}(A_g)$, respectively. The Raman spectrum can further confirms the identity of the as-prepared thin film as indeed $BaWO_4$.

Fig. 7 shows the room temperature PL spectra of the different microstructures using the same excitation line at 310 nm. The spectra show that both two samples exhibit emission peaks at about 390 nm which are consistent with the result reported by Jia et al. [39]. The strong emission peak corresponds to the highly crystallized thin film with compact cauliflower-like microstructure, while the relatively weak emission peak belongs to the thin film containing kernel-like microstructures with poor crystaillinity. The enhancement of PL intensity may be due to the improved crystallinity in the films, which was also observed by other researchers [40]. We also assume that the cauliflower-like crystals would possess more defects during the oriented aggregation process, so they possibly show more intense PL emission. The results could indicate that luminescence properties of $BaWO_4$ films are strongly dependent on the crystallinity and morphology.

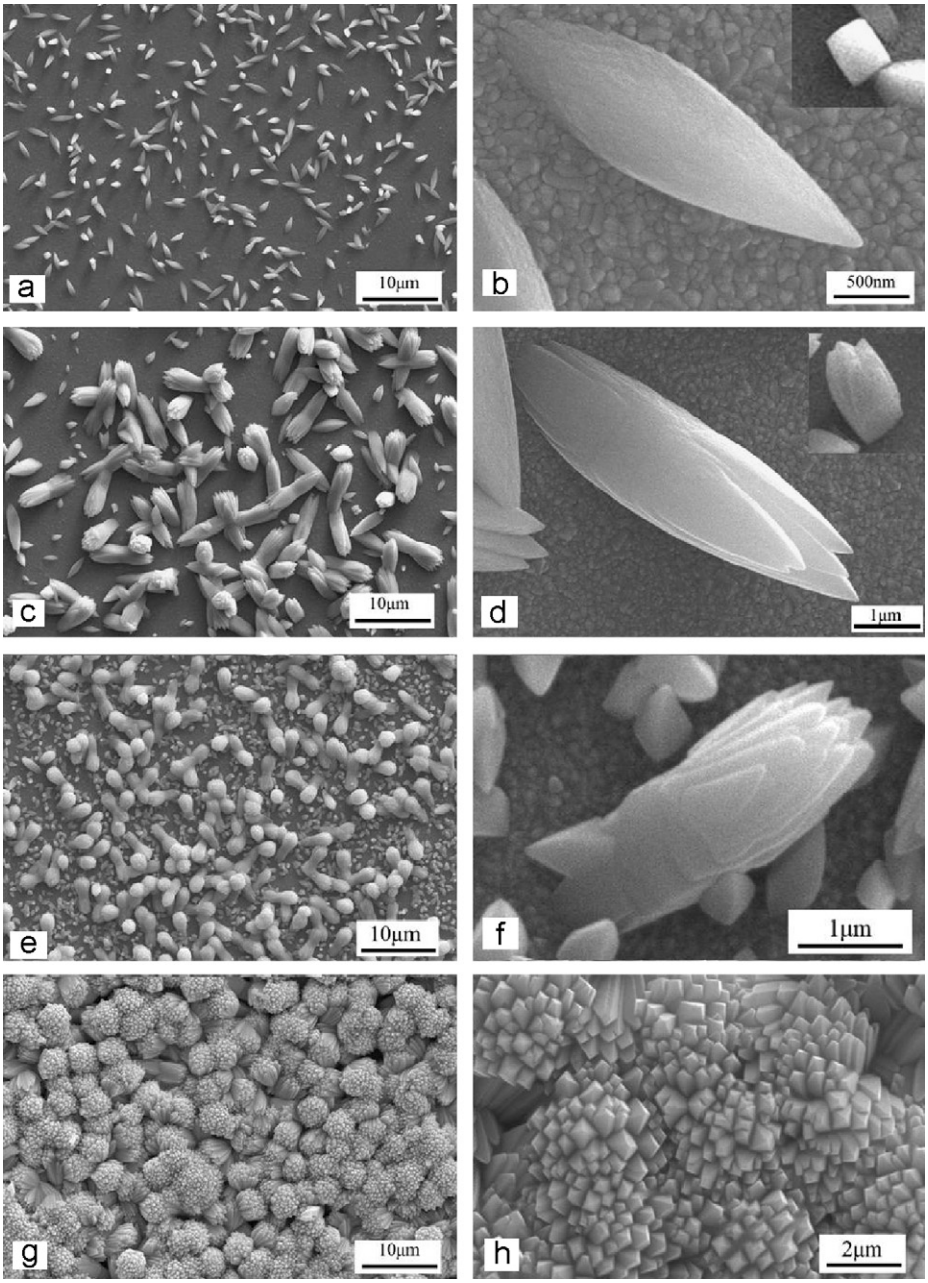


**Fig. 3.** SEM morphologies of the films on FTO coated glass substrate at different precursor concentration. ($[Ba^{2+}] = [EDTA] = [WO_4^{2-}]$ = (a, b) 0.05 M; (c, d) 0.1 M; (e, f) 0.2 M; (g, h) 0.3 M); pH = 8; 25 min.

## 4. Discussion

In this study, we successfully achieve the one-step rapid synthesis of $BaWO_4$ thin films with controllable microstructures through a bottom-up approach in an aqueous solution at relatively low temperature. To the best of our knowledge, a facile route to sheelite $ABO_4$-type ternary metal-oxide thin films with specific morphologies has not been demonstrated in earlier studies. A deep understanding of the formation process would lead to the widespread application to other $ABO_4$-type ternary metal oxide thin films.

It is clear that the growth of crystals is controlled by nucleation and growth processes in aqueous solution. The crystalline phase of the nuclei is critical for directing the intrinsic shapes of the crystals due to the characteristic symmetry and structure. In the subsequent stage, the crystal growth step is mainly a kinetically controlled process, during which the final microcrystallites undergo a successive morphological evolution process.

### 4.1. Nucleation process

#### 4.1.1. Effect of ligands

$BaWO_4$ with the formula $ABO_4$ (where *A* and *B* are two different metallic elements with oxidation states of +2 and +6, respectively) are characterized by the tetragonal space group $I4_1/a$ or $C_{4h}^6$ (Fig. 8). In this structure, the primitive unit cell is described to have two $ABO_4$ units [41], each of which has an inversion center. The *A* and *B* sites have S4 point symmetry.

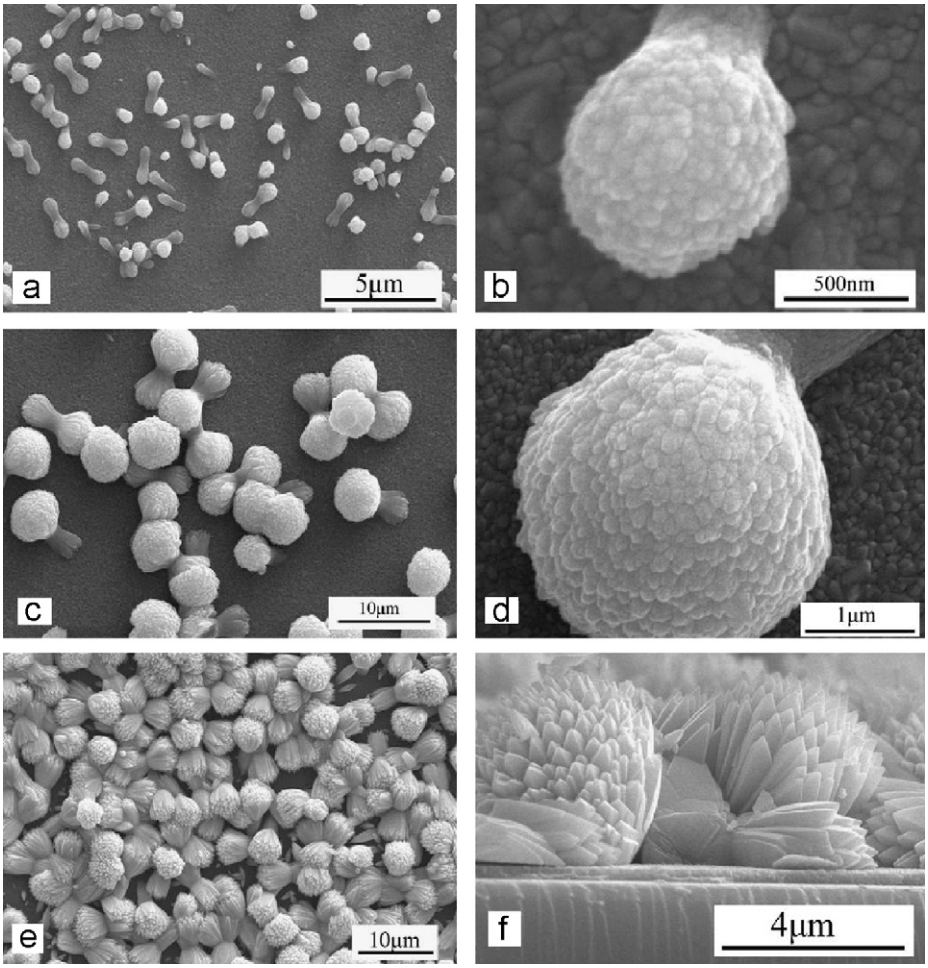


**Fig. 4.** SEM morphologies of films deposited on the FTO substrate at various times: (a,b) 2 min; (c,d) 6 min; (e) 16 min; (f) 25 min (precursor concentration = 0.3 M, pH = 8).

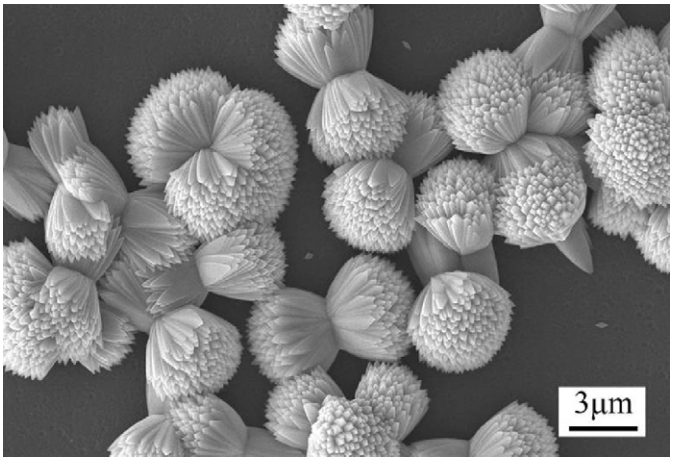


**Fig. 5.** SEM morphologies of films deposited on glass substrate: precursor concentration = 0.3 M; 25 min; pH = 13.

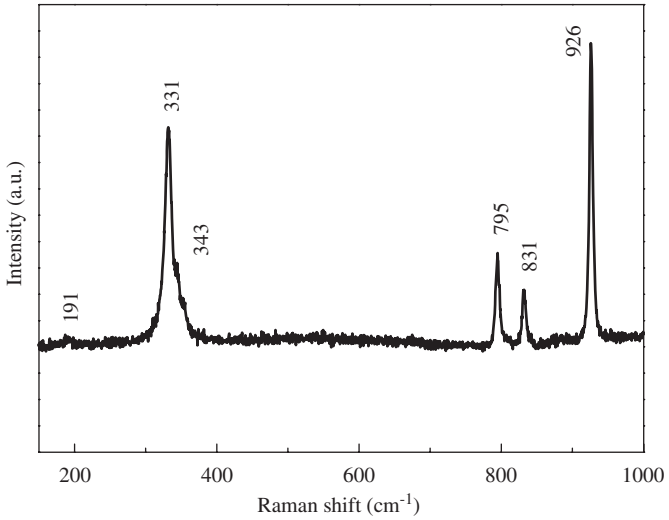


**Fig. 6.** Raman spectra of the films deposited on FTO substrate at a precursor concentration = 0.3 M, pH = 8, 25 min.

Organic ligands have a profound effect on the growth mechanism and physical properties of colloidal nanocrystals and microcrystals. The ligands also influence solubility and can affect the effective volume of the nanocrystals, their surface charge, and their ability to adhere to substrates, which may affect the deposition of films of nanocrystals and microcrystals [42]. The deprotonated EDTA contains six coordinating atoms (two amino N-donor atom and four carboxylic acid group O-atoms), it integrates $Ba^{2+}$ by forming five-member rings complex and eliminating available coordination sites [43].

Until now, the long axis of the elongated nanocrystals with a sheelite structure has been observed as the *c*-axis of the crystals [44,45]. One explanation for this particular orientation is based on the crystal structure and the surface coordination of the ligands.

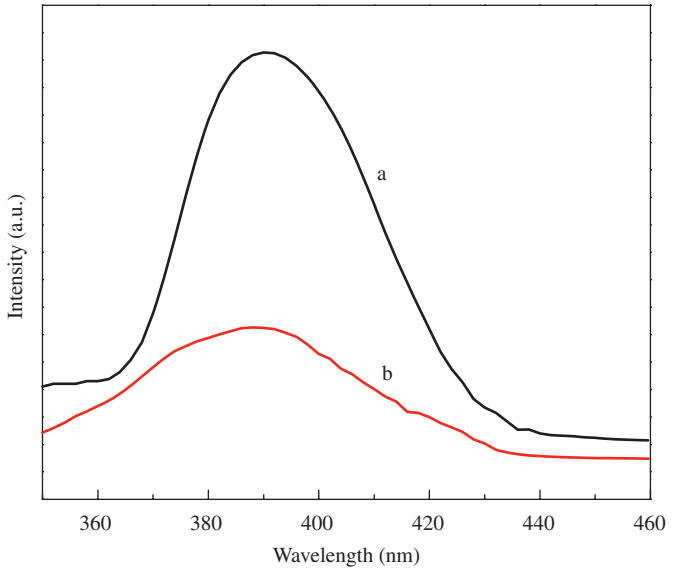


**Fig. 7.** Room-temperature PL spectra of $BaWO_4$ films: (a) precursor concentration = 0.2 M; 25 min; pH = 8; (b) precursor concentration = 0.05 M; 25 min; pH = 8.

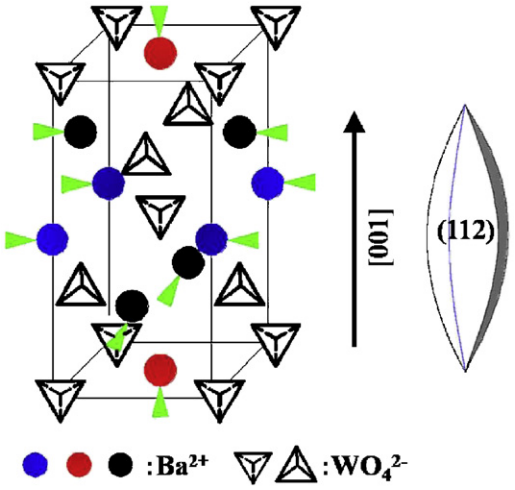


**Fig. 8.** Crystal structure of $BaWO_4$ and the proposed primary particle.

Since ligands in the system are for cationic species only, any cationic ion exposed on the surface with dangling bonds has a tendency of forming complex with the ligands. In this way, the morphology of primary particle is largely determined by the release rate of the complex. As shown in Fig. 8, four $Ba^{2+}$ embedded in the middle of the primitive unit surface and one $Ba^{2+}$ locates at both ends. The $EDTA^{2-}$ acts as Liews alkali to selectively stabilize nucleated active site (the exposed $Ba^{2+}$) and provides steric hindrance by the chelated rings. So, the less it attached on the facets, the more likely for free $WO_4^{2-}$ in the precursor solution to combined with $Ba^{2+}$ in the primary nuclei to form new nuclei and grow. Since the fastest growth facets disappear fastest, the end facets are more easily react with $WO_4^{2-}$ to grow and finally vanish. Simultaneity, the middle plane affected by large local ligand hindrance grows slowly, which keeps the middle part of the microcrystal relatively sturdy. Therefore, some "big in the middle and pointed in both ends" nano primary particles most probably appears at the beginning. Though, the very image of this stage was failed to be captured in this work, we still believe that the similar nanostructure exits and plays an important role in the final microstructures observed in Fig. 3a and b based on Shi's work [44]. Shi et al. carefully detected the nucleation process of penniform $BaWO_4$ nanostructures by TEM, and the *c*-axis-oriented shuttle-like nanocrystals with a few tens of nanometers length were clearly observed.

### 4.1.2. *Effect of FTO substrate*

It should be mentioned that the local maximum temperature during actual film growth on the F: $SnO_2$ substrate could be somewhat higher than 100 °C (water boiling temperature), due to localized heating of the conducting F: $SnO_2$ layer, originating from its interaction with microwaves [18]. Localized heating of the substrate is also thought to promote heterogeneous nucleation by sufficient energy source. Since nanocrystals act as effective crystallization promoter seeds to spawn crystal nuclei with the same structure by reducing the free-energy barrier [37,46], heterogeneous nucleation and growth process of $BaWO_4$ crystals can occur on the tetragonal FTO substrate more easily. Also, the F ions inserted in the $SnO_2$ lattices with the maximum electronegativity is more easily to cap free $Ba^{2+}$, then become the active spots for nucleation. Thus, quite a few nano-nuclei form on the FTO substrate and begin to grow in an upright direction. In contrast, parallel growth is mainly observed on the glass substrate, which probably because heterogeneous nucleation on the chemically inert glass surface is not as frequent as that on FTO, even though in the high concentration of precursor solution (0.3 M). Thus, the frequent nucleation on the FTO substrate and the seed-inducement effect result in the compact vertically standing microcrystals. The XRD patterns of the films on FTO substrates are shown in Fig. 9. In contrast to the XRD patterns of $BaWO_4$ films on glass substrate (as shown in Fig. 1), the relative intensity of (112) and (204) diffraction peak is remarkably strong, which is in good agreement with the vertically standing microstructure. Mechanisms for the orient growth on FTO substrate are still unclear, although the similar orientation behaviors were reported in the case of hydroxide zinc carbonate nanosheets [47], manganese oxide nanosheets [48], and zinc oxide nanorods [49].

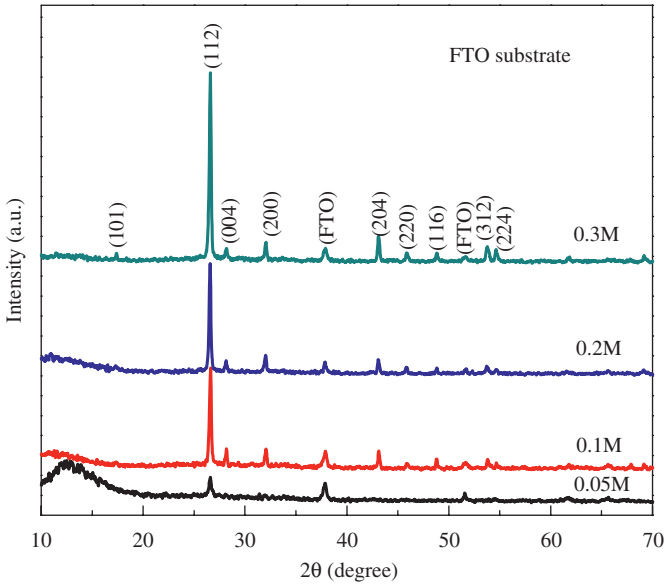


**Fig. 9.** XRD patterns of the as-prepared films on FTO substrate at different precursor concentration with the same pH value (pH = 8) and reaction time (25 min).

### 4.2. Growth mechanism and morphology evolution

From our experimental results, it is reasonable to presume that the formation of hierarchical $BaWO_4$ microstructure is based on the oriented aggregation mechanism, and the formation and evolution process can be divided into two general steps: the initial nucleating and oriented aggregation and the following growth and ripen process. Oriented aggregation mechanism has been proposed to explain the shaft forming process of the penniform $BaWO_4$ nanostructures where the shuttle-like nanocrystals aggregated by the attachment of parallel aligned forming [100]-oriented shaft with many parallel [001]-oriented pricks in a catanionic reverse micelles [44]. However, in our case, oriented aggregation process may occur most commonly on {112} and occasionally on {204} to form the kernel-like microstructure with four distorted (112) facets, as reported by Geng et al. in a similar case of $PbWO_4$ [45]. This process is thermodynamically favorable, since the surface energy is significantly reduced due to the elimination of the interface. Primary particles may aggregate in an oriented fashion to produce a large single crystal, or they may aggregate randomly and reorient, recrystallize, or undergo phase transformations to produce large single crystals [50,51]. This kind of growth mode could lead to the formation of faceted particles or anisotropic growth if there is sufficient difference in the surface energies of different crystallographic faces [52]. The rough surface of the microcrystals (Fig. 3b) also suggests that the four-side kernel-like $BaWO_4$ crystals are assembled by some primary particles.

#### 4.2.1. Effect of precursor concentration

Heterogeneous nucleation of $BaWO_4$ is very rapid, and the nuclei form either on the surface of substrate or the existent crystals in the initial stage. At a relatively low precursor concentration (0.05 M), sparse kernel-like rods finally form on the substrate. When the precursor concentration increases to 0.1 M, new nuclei prefer to aggregate onto existing rods to seek a relatively low energy. Then, the subsequent growth on crossed rods leads to the formation of multilayer bowknot-like rudiments. With further increase of the precursor concentration, more nuclei grow both at the substrate and on the existing microcrystals, due to the large supersaturation. The former starts to form other kernel-like rods and the latter adds the number of the "forks" which evolved from the middle part of the $BaWO_4$ rod. Fig. 10 clearly exhibits the coexistent of the tiny pricks and multilayer bowknot-like microcrystals. This indicates that the initial concentration of $Ba^{2+}$ and $WO_4^{2-}$ ions has an important influence on the final morphologies of the products. The possible growth routes of these as-prepared $BaWO_4$ microcrystals are schematically summarized in Fig. 11.

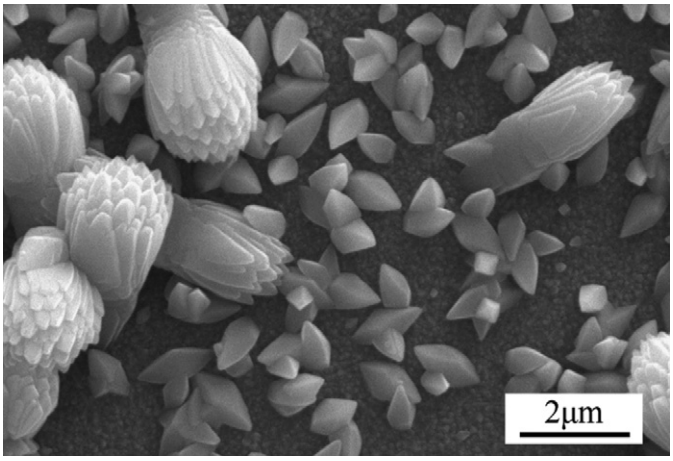


**Fig. 10.** SEM morphology of films deposited on FTO substrate at a precursor concentration of 0.2 M, 25 min, pH = 8.

## 5. Conclusion

Highly crystallized $BaWO_4$ thin films with controllable microstructures and orientation were firstly obtained by the presented facile and rapid synthesis route (MA-CBD) in alkalescent aqueous solutions. Possible nucleation and growth mechanisms of these thin films are discussed. It is found that final film morphologies are mainly controlled by anisotropic structure of $BaWO_4$, the precursor concentration and the activity of the substrates. In addition, our group had applied MA-CBD to deposit zircon structured ternary metal-oxide Eu: $YVO_4$ thin films [21]. Since $BaWO_4$ and $YVO_4$ are two representative $ABO_4$-type materials in structural and valence. It is anticipated that this simple, rapid and low-cost technique methodology can be generalized to deposit other types of $ABO_4$-type thin films with controllable morphologies, which is advantageous for practical application.

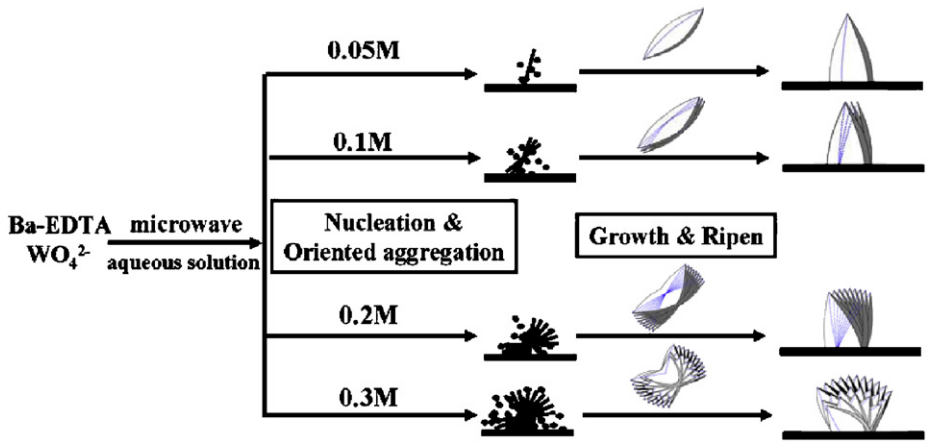


**Fig. 11.** Schematic illustration of the possible growth routes of these as-prepared $BaWO_4$ microcrystals on the FTO substrate.

## Acknowledgments

This work is supported by the Natural Science Foundation of Beijing (no. 4082008), Scientific and Technological Development Project of Beijing Education Committee (no. KM200710005029), and the Opening Project of State Key Laboratory of Green Building Materials (no. GBM-08-KF104).

## References

[1] A.P. Alivisatos, Science 271 (1996) 933–937.
[2] S. Mann, Angew. Chem. Int. Ed. 39 (2000) 3392–3406.
[3] S.H. Yu, M. Antonietti, H. Colfen, H. Jurgen, NanoLetters 3 (2003) 379–382.
[4] H.T. Shi, L.M. Qi, J.M. Ma, H.M. Cheng, J. Am. Chem. Soc. 125 (2003) 3450–3451.
[5] J.Y. Lao, J.G. Wen, Z.F. Ren, NanoLetters 2 (2002) 1287–1291.
[6] Y. Xia, P. Yang, Y. Sun, Y. Wu, B. Mayer, B. Gates, Y. Yin, F. Kim, H. Yan, Adv. Mater. 15 (2003) 353–389.
[7] S.H. Yu, H. Colfen, M. Antonietti, Chem. Eur. J. 8 (2002) 2937–2945.
[8] X.M. Sun, Y.D. Li, Chem. Eur. J. 9 (2003) 2229–2238.
[9] M. Li, H. Schnablegger, S. Mann, Nature 402 (1999) 393–395.
[10] Q. Peng, Y.J. Dong, Y.D. Li, Angew. Chem. Int. Ed. 42 (2003) 30273030.
[11] R. Zhang, L.L. Kerr, J. Solid State Chem. 180 (2007) 988–994.
[12] T.P. Niesen, M.R. De Guire, J. Electroceram. 6 (2001) 169–207.
[13] E. Vigil, L. Saadoun, J.A. Ayllon, X. Domenech, I. Zumeta, R. Rodriguez-Clemente, Thin Solid Films 365 (2000) 12–18.
[14] X.C. Xu, W.S. Yang, J. Liu, L.W. Lin, Adv. Mater. 3 (2000) 195–198.
[15] X.H. Liao, J.M. Zhu, J.J. Zhu, J.Z. Xu, H.Y. Chen, Chem. Commun. 10 (2001) 937–938.
[16] O. Palchik, J.J. Zhu, A. Gedanken, J. Mater. Chem. 10 (2000) 1251–1254.
[17] J.J. Zhu, O. Palchik, S.G. Chen, A. Gedanken, J. Phys. Chem. B 104 (2000) 7344–7347.
[18] A.M. Peiro, J.A. Ayllon, J. Peral, X. Domenech, C. Domingo, J. Crystal Growth 285 (2005) 6–16.
[19] R. Zhai, S.B. Wang, H.Y. Xu, H. Wang, H. Yan, Mater. Lett. 59 (2005) 1497–1501.
[20] I. Zumeta, R. Espinosa, J.A. Ayllon, E. Vigil, Semicond. Sci. Technol. 17 (2002) 1218–1222.
[21] H.Y. Xu, H. Wang, T.N. Jin, H. Yan, Nanotechnology 16 (2005) 65–69.
[22] M. Nikl, P. Bohacek, E. Mihokova, M. Kobayashi, M. Ishii, Y. Usuki, V. Babin, A. Stolovich, S. Zazubovich, M. Bacci, J. Lumin. Sci. 87–89 (2000) 1136–1139.
[23] P. Cerny, P.G. Zverev, H. Jelinkova, T.T. Basiev, Opt. Commun. 177 (2000) 397–404.
[24] P. Cerny, H. Jelinkova, Opt. Lett. 27 (2002) 360–362.
[25] A.K. Chauhan, J. Crystal Growth 254 (2003) 418–422.
[26] H.T. Shi, L.M. Qi, J.M. Ma, H.M. Cheng, Chem. Commun. (2002) 1704–1705.
[27] D. Li, H. Wu, Z. Li, X.F. Cong, J. Sun, Z.H. Ren, L.P. Liu, Y. Li, D.W. Fan, J.C. Hao, Colloids Surf. A Physicochem. Eng. 274 (2006) 18–23.
[28] X.F. Zhao, T.K. Li, Y.Y. Xi, H.L.N. Dickon, J.G. Yu, Cryst. Growth Des. 6 (2006) 2210–2213.
[29] X.M. Wang, H.Y. Xu, H. Wang, H. Yan, J. Cryst. Growth 284 (2005) 254–261.
[30] L.A. Wills, B.W. Wessels, D.S. Richeson, T.J. Marks, Appl. Phys. Lett. 60 (1992) 41–43.
[31] C. Feldman, J. Soc. Motion Pict. Eng. (1958) 455.
[32] Y. Kashiwakura, O. Kanehisa, Jpn. Pat. 1 (1989) 263188.
[33] G.X. Zhang, R.P. Jia, Q.S. Wu, Mater. Sci. Eng. B 128 (2006) 254–259.
[34] A. Bauger, J.C. Mutin, J.C. Niepce, J. Mater. Sci. (1983) 3041.
[35] P. Krtil, M. Yoshimura, J. Solid State Electrochem. 2 (1998) 321–327.
[36] W.S. Cho, M. Yoshimura, Jpn. J. Appl. Phys. Part 1 36 (1997) 5658–5662.
[37] A. Cacciuto, S. Auer, D. Frenkel, Nature 428 (2004) 404–406.
[38] P.J. Miller, R.K. Khanna, E.R. Lippincott, J. Phys. Chem. Solids 34 (1973) 533.
[39] R.P. Jia, G.X. Zhang, Q.S. Wu, Y.P. Ding, Appl. Phys. Lett. 89 (2006) 043112.
[40] M. Yu, J. Lin, J. Fang, Chem. Mater. 17 (2005) 1783–1791.
[41] Y. Zhang, N.A.W. Holzwarth, R.T. Williams, Phys. Rev. B 57 (1998) 12738–12750.
[42] W. Wang, S. Banerjee, S.G. Jia, M.L. Steigerwald, I.P. Herman, Chem. Mater. 19 (2007) 2573–2580.
[43] R. Zhai, R. Wang, H. Wang, M.K. Zhu, H. Yan, J. Phys. D: Appl. Phys. 40 (2007) 4039–4042.
[44] H.T. Shi, X.H. Wang, N.N. Zhao, L.M. Qi, J.M. Ma, J. Phys. Chem. B 110 (2006) 748–753.
[45] J. Geng, J.J. Zhu, H.Y. Chen, Cryst. Growth Des. 6 (2006) 321–326.
[46] K.E. Kelton, in: H. Ehrenreich, D. Turnbull, (Eds.) Solid State Physics, Academic Press, New York, 1991, p. 45.
[47] E. Hosono, S. Fujihara, I. Honma, H. Zhou, Adv. Mater. 17 (2005) 2091–2094.
[48] Y.Y. Oaki, H. Imai, Angew. Chem. Int. Ed. 46 (2007) 4951–4955.
[49] D.S. Boyle, K. Govender, P. O'Brien, Chem. Commun. (2002) 80–81.
[50] J.F. Banfield, S.A. Welch, H.Z. Zhang, T.T. Ebert, R.L. Penn, Science 289 (2000) 751–754.
[51] R.L. Penn, J.F. Banfield, Science 281 (1998) 969–971.
[52] R.L. Penn, G. Oskam, T.J. Strathmann, P.C. Searson, A.T. Stone, D.R. Veblen, J. Phys. Chem. B 105 (2001) 2177–2182.